Journal of the European Ceramic Society, Volume 37, Issue 4, April 2017, pp. 1459-1466
10.1016/j.jeurceramsoc.2016.12.021

Enhancement of pyroelectric properties of lead-free $0.94Na_{0.5}Bi_{0.5}TiO_3$-$0.06BaTiO_3$ ceramics by La doping

A.M. Balakt, C.P. Shaw and Qi Zhang*

School of Aerospace, Transport and Manufacturing, Cranfield University, Cranfield, Bedfordshire, MK43 0AL, UK

*q.zhang@cranfield.ac.uk

Abstract

Lead-free 0.94NBT-0.06BT-xLa ceramics at x = 0.0 – 1.0 (%) were synthesized by a conventional solid-state route. XRD shows that the compositions are at a morphotropic phase boundary where rhombohedral and tetragonal phases coexist. With increasing La^{3+} content pyroelectric coefficient (p) and figures of merits greatly increase; however, the depolarization temperature (T_d) decreases. p is 7.42 x 10^{-4} C.m^{-2}.$^{\circ}$C^{-1} at RT at x=0.5% and 105.4 x10^{-4} C.m^{-2} $^{\circ}$C^{-1} at T_d at x=0.2%. F_i and F_v show improvements at RT from 1.12 (x=0%) to 2.65 (x10 $^{-10}$ m.v^{-1}) (x=0.5%) and from 0.021 to 0.048 (m^2.C^{-1}) respectively. F_i and F_v show a huge increase to 37.6 x10-10 m.v-1 and 0.56 m2.C-1 respectively at Td at x=0.2%. FC shows values of 2.10, 2.89, and 2.98 (x10^{-9} C.cm^{-2}. $^{\circ}$C^{-1}) at RT at 33, 100 and 1000 (Hz) respectively. Giant pyroelectric properties make NBT-0.06BT-xLa at x=0.2% and 0.5% promising materials for many pyroelectric applications.

Keywords*: Lead free ceramics; Lanthanum doping NBT-0.06BT; Morphotropic phase boundary (MPB); Depolarization temperature; Pyroelectric properties; Figure of merits.*

1. *Introduction*

Lead-based ferroelectric ceramics with perovskite structure such as lead zirconate titanate (PZT) and PZT-based are widely utilized in diverse microelectronic devices, such as actuators,

transducers and sensors, because of their superior piezoelectric and pyroelectric properties. However, there are two serious environmental problems arising from the fabrication of lead-containing materials: atmospheric pollution caused by PbO vapour during ceramic fabrication, and the difficulty in removing lead during component recycling [1]. Thus, there is a high demand to find lead-free alternatives which can fill the industrial gap of the lead-based materials in a wide range of applications.

Sodium bismuth titanate, $Na_{0.5}Bi_{0.5}TiO_3$ (NBT), is a lead-free ferroelectric ceramic with perovskite structure. It shows a large remnant polarization (P_r=38 μC.cm^{-2}) and a high Curie temperature (T_c = 320 $^{\circ}$C). Additionally, it has two structural phase transitions, from rhombohedral (*R*) to tetragonal (*T*) between 200 $^{\circ}$C - 320 $^{\circ}$C and from tetragonal (*T*) to cubic (*C*) between 500 $^{\circ}$C - 540 $^{\circ}$C [2–6]. The first phase transition has been widely discussed but its origin is still being debated. It either has morphotropic phase boundary (*MPB*) where both phases (*R* and *T*) with nanopolar regions coexist or changes to *T* as antiferroelectric (AFE) [2-6]. The NBT shows first anomaly at ~ 200 $^{\circ}$C and starts losing its ferroelectric properties with further increasing temperature. This temperature is defined as the depolarization temperature (T_d) [6]. However, the high coercive field (E_c = 73 kV.cm^{-1}) at room temperature (*RT*) makes NBT very difficult to be fully polarized [2-6]. NBT ferroelectric, piezoelectric and pyroelectric properties can be improved by two ways: (1) NBT-based material combines with a second oxide such as $BaTiO_3$, $NaNbO_3$, $Bi_{0.5}K_{0.5}TiO_3$, $SrTiO_3$, and many other compositions [3,5,7]forming a ceramic solid solution. Among these systems, (1-x) $Na_{0.5}Bi_{0.5}TiO_3$-x$BaTiO_3$ (NBT-xBT) has been intensively studied and considered as one of the most promising systems for piezoelectric and pyroelectric applications, in particular, at a morphotropic phase boundary (*MPB*) composition at x = 0.06-0.07 [8,9] because NBT-xBT is much easier to pole than NBT and also it shows a large improvement in its properties due to the coexistence of rhombohedral

and tetragonal; (2) doping with other oxides such as MnO_2, Eu_2O_3, La_2O_3 etc. has also been proved to be effective [7].

Although the ferroelectric, dielectric and piezoelectric properties of undoped and doped NBT-xBT have been intensively investigated [10,11] their pyroelectric properties were studied relatively much less [4]. Depolarization temperature (T_d) is one of the most important characters in the pyroelectric studies but its origin and function in pyroelectric properties have not been fully understood, though it was reported in the literature [4,5]. Felix *et al*. investigated the pyroelectric behavior and the dielectric constant at microwave frequency (10MHz to 3GHz) of NBT-xBT ($0.04 \leq x \leq 0.06$). They concluded that the pyroelectric properties of NBT-xBT at MPB ($x = 0.06$) were better than those at $x = 0.04$. Also its pyroelectric coefficient (p) was comparable to that of PZT material [12]. Abe *et al*, studied the pyroelectric properties of NBT-0.06BT ceramics doped with MnO_2 and reported that the pyroelectric coefficient (p) value is 3.5×10^{-4} C.m^{-2}.$^{\circ}$C^{-1} at RT [13]. Ruiz *et al*. studied the pyroelectric properties of NBT-0.065BT. They found that the pyroelectric coefficient is equal to 4.6×10^{-4} C.m^{-2}.$^{\circ}$C^{-1} at RT [14]. Guo *et al*. studied the pyroelectric properties of Zr-doped NBT-x$BaTO_3$ ($0 \leq x \leq 0.12$) ceramics and found that the pyroelectric coefficient of this composition was enhanced from 5.7 C. m^{-2}.$^{\circ}$C^{-1} at RT to 22.1 C.m^{-2}.$^{\circ}$C^{-1} at T_d (87 $^{\circ}$C) [4]. Balakt et al. investigated the effects of Ba^{2+} content on the pyroelectric properties of NBT-0.06BT ceramics [15]. They found that p increases from 2.90 to 3.54 (x10^{-4} C.m^{-2}.$^{\circ}$C^{-1}) at RT when $x = 1.02$. In addition, the p shows huge enhancement from 55.3 to 740.7 (x10^{-4} C.m^{-2}.$^{\circ}$C^{-1}) at Td for composition NBT-0.06B1.02TiO3 [15].

In this study, the pyroelectric properties of La_2O_3 doped NBT-0.06BT were investigated with the aim to bring down the T_d to near RT and simultaneously, to improve the pyroelectric properties at both RT and T_d.

2. *Experimental*

A solid state synthesis route was selected to prepare La^{3+}-doped 0.94NBT-0.06BT composition. The raw materials used in this project were powders, lithium oxide (La_2O_3), 99.5%, bismuth oxide (Bi_2O_3), 99.999%, sodium carbonate (Na_2CO_3), 99.5%, barium carbonate ($BaCO_3$), 99.98%, and Titanium dioxide (TiO_2), > 99.8% (all Sigma- Aldrich).

The amounts of powders were calculated according to the chemical formula of $0.94Na_{0.5}Bi_{0.5}TiO_3$-$0.06BaTiO_3$-$xLa_2O_3$, with x= 0.0, 0.2%, 0.5%, and 1.0%. The raw materials were ball-milled (zirconia milling media) in acetone for 24 hrs. to reduce the particle size of the powders. The resultant slurries were dried at 50 °C overnight. The dried powder cakes were ground in a mortar for 10 min. and sieved through a 250 μm mesh. and then calcined at 850 °C for 180 min. in a closed alumina crucible at a heating ramp rate of 1°C per minute and cooling rate 5 °C per minute. After calcination powders were re-milled for 24 hrs. in acetone, to make more reduction of the particle size of the powder. Then 2 % of poly vinyl alcohol (PVA) was added as an organic binder to enhance the mechanical strength of the particles. After that the powders were dried in an oven at 80 °C until fully dried. The dried powders were ground and sieved and subsequently pressed into green pellets with a diameter of 10 mm under a uniaxial compaction with a load of ~78 MPs for 5 min at RT. The pellets were sintered at temperatures up to 1150 °C in closed crucibles in order to minimize the loss of volatile Na^+ and Bi^{3+} for 120 min. The pellets were polished in both sides and thermally etched for 30 min. at 1000 °C for macrostructure study. SEM (FEI XL30 SFEG) was used to look at the grain morphology of the sintered samples and X-Ray Diffraction (XRD) (Siemens Ltd Model: D500) was used to investigate their crystallisation and phase structure. Silver conductive paint (RS limited) was used to electrode the pellets, and electrical poling at 6.5 kV/mm for 10 min at RT in silicone oil was carried out using a Keithley (6517 Electrometer/high resistance) dc power supply.

Dielectric measurements were made using an impedance analyser (Wayne kerr Electronics Ltd. Model 3245 and Hewlett Packard HP4092A)) over a temperature range from RT to 150 °C in

a frequency range of 0.1 - 10 kHz. Pyroelectric measurements were made using the Byer-Roundy [16] method on a custom-built computer controlled rig which used a thermoelectric heater to ramp the temperature between 20°C and 90°C under vacuum and the pyroelectric current was collected with a Keithley electrometer (Model 6217). Dielectric and pyroelectric data was then used to study the phase changes such as depolarization temperatures (T_d), and to determine figure of merit values F_i, $F_{v,}$ F_D and F_C.

3. *Results and discussion*

3.1 *Effects of La^{3+} on microstructure*

Fig.1 (a) shows X-ray diffraction patterns of the La-doped NBT-0.06BT ceramic pellets sintered at 1150 °C for 2 hrs. All samples showed a pure perovskite structure (ABO_3), indicating that the NBT-0.06BT lattices have absorbed the La^{3+} content forming a new solid solution, NBT-0.06BT-xLa [4,12,13,17–19]

Lattice parameters (Å) and c/a ratio of all the samples are given in Table 1. Table 1 shows that the lattice parameters "a = b" and "c" are affected by La^{3+} doped. The c/a ratio shows that Sample B has the lowest ratio among all the samples. La^{3+} can substitute A-site ions in NBT-0.06BT due to the radius similarity according to the Shannon radii [12,13,20–24].

Fig.1 (b) shows that a split of the peak [111] into [003] and [021] at 39.0° to 41.0° for all the samples as shown in undoped NBT [3,21,25,26], indicating the existence of rhombohedral phase. Another split was observed in [200] into [200] and [002] at 46.0° - 48.0°, which indicates the existence of tetragonal phase in NBT lattice (Fig. 1(c)). The coexistence of rhombohedral and tetragonal phases in NBT-0.06BT-xLa ceramics verifies that all the compositions are at morphotropic phase boundary (*MPB*) region. The coexistence of rhombohedral and tetragonal in NBT-xBT at x = 0.06-0.07 was reported in literature [4,20,22,27]. Therefore, the NBT-0.06BT-xLa phase structure (Sample A-D) is consistent with that reported in literature [15, 22, 24, 28, 29].

Fig. 2 exhibits the SEM morphology of all the NBT-0.06BT-xLa ceramic samples. Sample A presents a quite dense structure with a few visible pores. The structures of Samples B, C, and D become denser and no obvious pores can be identified. Sample A presents two distinguishable grain shapes, rod and granule in a wide range of sizes. However, after La^{3+} doping, the granules disappeared and only rods with different sizes existed. The average grain size varies with La^{3+} content and shows a sharp increase firstly from 1.78 μm (x = 0.0 %) to 2.85 μm (x = 0.2 %) then slightly decrease to 2.71 μm (x = 0.5 %) then further to 2.59 μm (x =1.0 %). Sample B presents the biggest grain size among all other samples. La^{3+} enhances the growth of NBT-0.06BT-xLa grains when it substitutes Na^{+}, resulting in A-site vacancies in order to keep charge balance. Generally, the creation of the A-site vacancies is quite beneficial for the mass transportation. This mass transport might be responsible for boosting the grain growth in the NBT-0.06BT-xLa with increasing La^{3+} concentration [12,25].

The densities of Samples B, C, and D (5.841, 5.785, and 5.845 ($gm.cm^{-3}$), respectively) are quite similar but higher than that of Sample A (5.757 $gm.cm^{-3}$). The higher densities of the doped samples are supported by the SEM pictures (Fig. 2).

3.2 *Effects of La^{3+} on dielectric properties*

Fig. 3 shows the temperature dependence of dielectric properties of poled NBT-0.06BT-xLa, from RT up to 150°C at 1, 10, and 100 kHz.

The undoped sample shows a relative permittivity (ε_r) value of ~ 400 at RT and 1 kHz (Fig. 3 a) whereas the doped samples present higher ε_r values of 600 – 700 (Fig.3 b to d). The ε_r of all the samples increased with temperature, which is typical for ferroelectric materials [28]. The relative permittivity against temperature demonstrates an obvious declining (Fig 4(a)). This declining temperature starts at ~70, ~69 and ~30 °C for x= 0.2, 0.5 and 1.0 (%), respectively but it was not identified for Sample A, (Fig4 (a)) although there is evidence that it may be outside the temperature measurement window. These temperatures are so close to the

temperatures where their dielectric losses (*tanδ*) show the maximum values which are around 75, 70, and 25 °C for samples B, C, and D, respectively (Fig 4(b)). These temperature values can be identified as depolarization temperatures (Td) (Fig 4(b)). The εr values for doped samples at Td, (1 kHz) are around 650 for Sample C and ~700 for Samples B, D. Sample D shows the highest relative permittivity value ~1300 at 150 °C, at which it was around 850 for sample A.

The increase in εr for doped samples with temperature is because the lattice deformation due to the La^{3+} substitution to Bi^{3+}. This deformation was identified by XRD (Table 1), which makes the ferroelectric domains re-orientating easier during the poling process. Bismuth in NBT-xBT volatiles at high temperature resulting in a higher conductivity or increasing the leakage currents [21]. As a result, La^{3+} addition to NBT-0.06BT leads to the increase of $\boldsymbol{\varepsilon_r}$ values [12,25]. La^{3+} can also substitute Na^{+}, which behaves as a donor, resulting in A-site vacancies and the increase of $\boldsymbol{\varepsilon_r}$ [12,29].

Dielectric losses (*tanδ*) of the doped samples are quite similar, which are between 0.055-0.06 at RT and 1 kHz, higher than the undoped sample (~0.04). Also the tanδ increased with temperature up to a certain value depending on the dopant content and then decreased. The maximum dielectric loss was observed at T_d, which is ~0.07, ~0.065, and ~0.055 for Samples B, C, and D respectively while it is around 0.05 for Sample A.

3.3 *Effects of dopant La^{3+} on depolarization temperature*

The T_d represents one of the important parameters in the pyroelectric study. It has a few definitions, and one of them is the phase transition temperature from ferroelectric (*FE*) to anti-ferroelectric (*AFE*) or to relaxor anti-ferroelectric (*relaxor-AFE*) phases [19,26,30–36].

In this study, the T_d were identified by two methods: 1. Dielectric method, the temperature at dielectric peak (Fig. 4 (a, and b)); 2. Pyroelectric method, the temperature at pyroelectric coefficient (p) peak (Fig. 5) [13]

The dielectric (permittivity& loss) vs temperature plots in Fig.4 reveal that T_d decreased from 115 °C (Sample A) to around 25 °C ~ 30 °C (Sample D) (Fig. 4 (a and b)), which is in agreement with the literature [25,35,37,38]. The T_d values identified from dielectric permittivity for the doped samples are slightly higher than or equal to the T_d identified from the dielectric loss ($tan\delta$) curves (Fig.4 (b)).

T_d can also be obtained from the ultimate pyroelectric coefficient values. It is known that the maximum p can be achieved at the phase transition temperature [20,26,32,35,37,39–42]. The T_d values identified by this method show a reduction in T_d from > 90 °C to ~ 67.9, ~ 73.5, and ~ 46.8 °C for Samples B-D respectively (Fig. 5). Sample C shows an abnormal T_d which is 6.0 °C higher than the T_d of Sample B as it should shift to lower temperature with increasing the dopant content (Fig. 5). The exact depolarization temperature could not be identified for Sample A by this method due to the maximum temperature of the equipment being at 90 °C (Fig 5).

The reason that T_d shifts to lower temperature with the increase of La^{3+} content might be because La^{3+} (1.36 Å) is larger than Bi^{3+}(1.31 Å). Generally, doping A-site of NBT-0.06BT with larger elements will shift T_d to lower temperature. Therefore, doping Sr, La and other elements in NBT-0.06BT [20,26,42–45] leads the T_d to lower temperatures, whereas, doping NBT-0.06BT with smaller elements such as Dy^{3+}(0.912 Å)[45–47] shifts the T_d value to higher temperature [45,46,48].

3.3 *Effects of La^{3+} on pyroelectric properties*

The pyroelectric coefficient (p) represents an important parameter for selecting the material for pyroelectric applications but improving the performance of a pyroelectric material cannot be achieved by only increasing the p value. Figure of merit (FOM) is another important parameter to be taken into account [13,21].

There are several types of FOMs depending on the special pyroelectric applications such as infrared or thermal imaging [12,18,25].

In this study, the pyroelectric coefficient (p) of NBT-0.06BT-xLa, 0.0 ≤ x ≤ 1.0 (%) was measured at RT and at 90 °C for Sample A or T_d for Samples (B, C, and D). The calculations of FOMs were calculated using Equations (2- 6) [4, 15, 17]:

$$I_p = pA\frac{dT}{dt} \qquad (2)$$

$$F_i = \frac{p}{C_v} \qquad (3)$$

$$F_v = \frac{p}{C_v \varepsilon_o \varepsilon_r} \qquad (4)$$

$$F_D = \frac{p}{Cv\sqrt{\varepsilon_o \varepsilon_r \ tan\delta}} \qquad (5)$$

$$F_C = \frac{p}{\sqrt{\varepsilon_r}} \qquad (6)$$

where T is absolute temperature, t the time, p the pyroelectric coefficient, Ip the pyroelectric current, F_i the FOM of the high current (i) detectivity, F_v the FOM of the high voltage (v) detectivity, F_D the FOM of the high and specific detectivity, F_C the FOM of the infrared detector materials, C_v* the specific heat (2.8 $JK^{-1}cm^{-3}$, quoted from [13]), ε_r the relative dielectric permittivity and ε_o the permittivity of free space.

Fig. 5 shows the change of p with temperature for NBT-0.06BT-xLa from 20 to 90 °C. Sample C (x = 0.5%) shows the highest p at RT. Samples B and C show similar profiles differentiated only by their own relative T_d values which coincide with the maximum observed p values for the samples. The T_d value for Sample A clearly lies outside the measurement window so it is difficult to comment on its likely profile. Sample D presents quite different profile with a broad shape; however, it shows the T_d, without distinguishable sharp peak. This profile may link to its structure and polarization states. Sample D composition is located at MPB. With the increase of temperature, the structure and polarization states possibly changed from rhombohedral and

tetragonal co-existing (MPB) ferroelectric to tetragonal ferroelectric and then to tetragonal antiferroelectric or relaxer. This phase transition may give the profile of the pyroelectric coefficient a broad and flat shape.

Pyroelectric coefficient (p) and FOMs F_i, F_v, and F_D values for all the samples at RT are listed in Table 2 and at 90 °C or T_d in Table 3.

The p increased from Samples A to D at RT and a huge increase at T_d. Sample C has the highest p value at RT while Sample B at T_d, which probably links to the microstructure change of these samples. The calculation of c/a ratio reveals that Sample C has a higher ratio which means that Sample C has more tetragonality in its structure than Sample B at RT (Table 1).

The huge increase in p at T_d may be attributed to the positive correlation between p and pyroelectric current (I_p), which reaches the maximum at T_d [18]. The large p values obtained at Td are most likely related to a phase transition. The T_d coincides with the phase transition temperature. At RT and at T_d, the p values for Samples B and C are higher than those of PZT and other lead-free ceramic compositions (Tables 2 and 3) [5,20,35,39].

The F_i and F_v values show an increase from Samples A to D at RT and a large increase at T_d due to their large p values. Comparing the F_i and F_v values with those of PZT and other lead-free ceramic compositions at RT, the La-doped NBT-0.06BT samples have higher F_i and F_v (Tables 2 and 3).

F_D values of all doped samples at RT and 90°C or T_d show worse values. The lower F_D values for doped samples may be related to the higher values of both relative permittivity and the dielectric loss which are higher than the undoped sample, though pyroelectric coefficient values of Samples B, C, and D were quite higher than Sample A value.

The F_C values of NBT-0.06BT-xLa at RT and at 33, 100, 1000 (Hz) were calculated. Generally, the materials suitable for infrared detectors should have the FC threshold value at ~ $3\pm1 \times 10^{-9}$ C. cm^{-2}.°C^{-1} [14]. The composition of Sample C presents F_C values 2.10 ± 0.380, 2.89

± 0.398, and 2.98 ± 0.205 (x 10^{-9} C.cm^{-2}. $^{\circ}C^{-1}$) at RT and at 33, 100, 1000 (Hz) respectively, which are suitable for infrared detectors. However, Samples A, B, and D show the F_C values less than the threshold value. RodrÍguez-Ruiz et al [14]. investigated the pyroelectric coefficient of 0.935Na0.5Bi0.5TiO3-0.065BaTiO3 ceramics and calculated the F_C of this material which equals to 1.44 x10^{-9} C.cm^{-2}. $^{\circ}C^{-1}$, which is also lower than the threshold value. The high F_C values for Sample C in this work are due to the high p and the lower relative permittivity at RT.

4. *Conclusion*

La-doped lead-free NBT-0.06BT ceramics were prepared using a conventional solid state technique. The pyroelectric properties of these compositions were investigated and compared with undoped NBT-0.06BT and other lead-free materials including PZT.

All compositions were found being at the morphotropic phase boundary area. The values of lattice parameters and c/a ratio slightly changed with increasing the dopant content. The average grain size, relative permittivity (ε_r) and dielectric loss ($tan\delta$) increase with La content. The T_d was identified by two different ways and decreases from ~ 115 $^{\circ}$C in NBT-0.06BT to RT and 46.8 $^{\circ}$C in 1.0 % La-doped NBT-0.06BT, according to the dielectric and pyroelectric coefficient methods respectively.

Samples B and C show the optimum p, F_i and F_v values at RT and at T_d respectively. Sample C shows F_C values of 2.10, 2.89, and 2.98 (x10^{-9} C.cm-2. $^{\circ}C^{-1}$) at RT at 33, 100 and 1000 (Hz) respectively which are suitable for infrared detectors. The results presented in this study demonstrate that NBT-0.06BT-xLa ($0.2\% \leq x \leq 0.5\%$) ceramics are promising materials for infrared detectors and other pyroelectric applications in a wide temperature range.

References

[1] G.G. Notes, Sustainable development and Environment EC Directive on WEEE and ROHS in electrical and electronic equipment, (2005).

[2] S.Y. Cheng, J. Shieh, H.Y. Lu, C.Y. Shen, Y.C. Tang, N.J. Ho, Structure analysis of bismuth sodium titanate-based A-site relaxor ferroelectrics by electron diffraction, J. Eur. Ceram. Soc. 33 (2013) 2141–2153. doi:10.1016/j.jeurceramsoc.2013.03.020.

[3] K.A. Razak, C.J. Yip, S. Sreekantan, Synthesis of (Bi0.5Na0.5)TiO3 (BNT) and Pr doped BNT using the soft combustion technique and its properties, J. Alloys Compd. 509 (2011) 2936–2941. doi:10.1016/j.jallcom.2010.11.163.

[4] F. Guo, B. Yang, S. Zhang, F. Wu, D. Liu, P. Hu, Y. Sun, D. Wang, W. Cao, Enhanced pyroelectric property in (1–x)(Bi0.5Na0.5)TiO3-xBa(Zr0.055Ti0.945)O3: Role of morphotropic phase boundary and ferroelectric-antiferroelectric phase transition, Appl. Phys. Lett. 103 (2013) 182906. doi:10.1063/1.4828675.

[5] S.T. Lau, C.H. Cheng, S.H. Choy, D.M. Lin, K.W. Kwok, H.L.W. Chan, Lead-free ceramics for pyroelectric applications, J. Appl. Phys. 103 (2008) 10–13. doi:10.1063/1.2927252.

[6] J. Suchanicz, U. Lewczuk, K. Konieczny, Effect of Ba doping on the structural, dielectric and ferroelectric properties of Na 0.5 Bi 0.5 TiO 3 ceramics, Ferroelectrics. 497 (2016) 85–91. doi:10.1080/00150193.2016.1163218.

[7] L.Y. Liu, M.K. Zhu, Y.D. Hou, H. Yan, R.P. Liu, Abnormal piezoelectric and dielectric behavior of 0.92Na0.5Bi0.5TiO 3-0.08BaTiO 3 induced by La doping, J. Mater. Res. 22 (2007) 1188–1192. doi:Doi 10.1557/Jmr.2007.0173.

[8] R. McQuade, M.R. Dolgos, A review of the structure-property relationships in lead-free piezoelectric (1-x)Na0.5Bi0.5TiO3-(x)BaTiO3, J. Solid State Chem. 3 (2015) 1–8. doi:10.1016/j.jssc.2016.01.008.

[9] C. Ma, X. Tan, Phase diagram of unpoled lead-free – ceramics, Solid State Commun.

150 (2010) 1497–1500. doi:10.1016/j.ssc.2010.06.006.

[10] Q. Zheng, C. Xu, D. Lin, D. Gao, K.W. Kwok, Piezoelectric and ferroelectric properties of (Bi0.94– x La x Na0.94)0.5 Ba0.06 TiO3 lead-free ceramics, J. Phys. D. Appl. Phys. 41 (2008) 125411. doi:10.1088/0022-3727/41/12/125411.

[11] H. Li, C. Feng, W. Yao, Some effects of different additives on dielectric and piezoelectric properties of (Bi1/2Na1/2)TiO3–BaTiO3 morphotropic-phase-boundary composition, Mater. Lett. 58 (2004) 1194–1198. doi:10.1016/j.matlet.2003.08.034.

[12] F.L. Martínez, J. Hinojosa, G. Doménech, F.J. Fernández-luque, J. Zapata, R. Ruiz, L. Pardo, Dielectric Constant Tunability at Microwave Frequencies and Pyroelectric Behavior, IEEE Trans. Ultrason. Ferroelectr. Freq. Control. 60 (2013) 1595–1602. doi:10.1109/TUFFC.2013.2740.

[13] M. Abo, Jiro Kobune, T. Nishimura, T. Yazaw, Y. Nakai, Effects of manganese addtion on pyroelelctric properties of (Bi0.5 Na0.5 TiO 3) 0.94 (BaTiO3) 0.06 ceramics, Integr. Ferroelectr. 80 (2006) 87–95. doi:10.1080/10584580600656502.

[14] R. RodrÍguez-Ruiz, R. González-Ballesteros, A. Flores-Cuautle, E. Suaste-Gómez, Determination of the Pyroelectric Coefficient for (Bi0.5 Na0.5) 0.935 Ba 0.065 TiO3 Piezoelectric Ceramics, Ferroelectrics. 368 (2008) 216–223. doi:10.1080/00150190802368537.

[15] A.M. Balakt, C.P. Shaw, Q. Zhang, The effects of Ba2+ content on depolarization temperature and pyroelectric properties of lead-free 0.94Na0.5Bi0.5TiO3 - 0.06Ba1+xTiO3 ceramics, J. Mater. Sci. Mater. Electron. 27 (2016) 12947–12954. doi:10.1007/s10854-016-5433-1.

[16] R.L. Byer, C.B. Roundy, Pyroelectric coefficient direct measurement technique and

application to a nsec response time detector, IEEE Trans. Sonics Ultrason. 19 (1972) 333–338. doi:10.1109/T-SU.1972.29679.

[17] Y. Guo, M. Gu, H. Luo, Antiferroelectric phase and pyroelectric response in (NayBi z)Ti1-xO3(1-x)-xBaTi3 ceramics, J. Am. Ceram. Soc. 94 (2011) 1350–1353. doi:10.1111/j.1551-2916.2011.04509.x.

[18] S. Patel, A. Chauhan, S. Kundu, N.A. Madhar, B. Llahi, R. Vaish, K.B.R. Varma, Tuning of dielectric, pyroelectric and ferroelectric properties of 0.715Bi0.5Na0.5TiO3-0.065BaTiO3-0.22SrTiO3 ceramic by internal clamping, AIP Adv. 5 (2015) 87145. doi:10.1063/1.4929328.

[19] S.G. Lee, C. Il Kim, B.C. Kim, Dielectric properties of screen-printed (Ba,Sr,Ca)TiO3 thick films modified with Al2O3 for microwave device applications, J. Eur. Ceram. Soc. 24 (2004) 157–162. doi:10.1016/S0955-2219(03)00252-8.

[20] M. Chen, Q. Xu, B. H. Kim, B. K. Ahn, J. H. Ko, W.J. Kang, O. J. Nam, Structure and electrical properties of (Na0.5Bi0.5)1-xBaxTiO3 piezoelectric ceramics, J. Eur. Ceram. Soc. 28 (2008) 843–849. doi:10.1016/j.jeurceramsoc.2007.08.007.

[21] J.H. Cho, Y.-H. Jeong, J.-H. Nam, J.-S. Yun, Y.-J. Park, Phase transition and piezoelectric properties of lead-free (Bi1/2Na1/2)TiO3–BaTiO3 ceramics, Ceram. Int. 40 (2014) 8419–8425. doi:10.1016/j.ceramint.2014.01.051.

[22] Q. Li, J. Wang, L. Ma, H. Fan, Z. Li, Large electrocaloric effect in (Bi0.5Na0.5)0.94Ba0.06TiO3 lead-free ferroelectric ceramics by La2O3 addition, Mater. Res. Bull. 74 (2016) 57–61. doi:10.1016/j.materresbull.2015.10.010.

[23] R.D. Shannon, Revised effective ionic radii and systematic studies of interatomic distances in halides and chalcogenides, Acta Crystallogr. Sect. A. 32 (1976) 751–767.

doi:10.1107/S0567739476001551.

[24] C. Xu, D. Lin, K.W. Kwok, Structure, electrical properties and depolarization temperature of (Bi0.5Na0.5)TiO3–BaTiO3 lead-free piezoelectric ceramics, Solid State Sci. 10 (2008) 934–940. doi:10.1016/j.solidstatesciences.2007.11.003.

[25] S. Anem, K. S. Rao, K. H. Rao, Investigation of lanthanum substitution in lead-free BNBT ceramics for transducer applications, Ceram. Int. (2016). doi:10.1016/j.ceramint.2016.06.173.

[26] M. Rawat, K.L. Yadav, A. Kumar, P.K. Patel, N. Adhlakha, J. Rani, Structural, dielectric and conductivity properties of Ba2+ doped (Bi0.5Na0.5)TiO3 ceramic, Adv. Mater. Lett. 3 (2012) 286–292. doi:10.5185/amlett.2012.2322.

[27] S. R. Kanuru, K. Baskar, R. Dhanasekaran, Synthesis, structural, morphological and electrical properties of NBT–BT ceramics for piezoelectric applications, Ceram. Int. 42 (2016) 6054–6064. doi:10.1016/j.ceramint.2015.12.162.

[28] Y. Hiruma, H. Nagata, T. Takenaka, Formation of Morphotropic Phase Boundary and Electrical Properties of (Bi1/2 Na1/2)TiO3 –Ba(Al1/2 Nb1/2)O3 Solid Solution Ceramics, Jpn. J. Appl. Phys. 48 (2009) 09KC08. doi:10.1143/JJAP.48.09KC08.

[29] R. Ranjan, A. Dviwedi, Structure and dielectric properties of (Na0.50Bi0.50)1−xBaxTiO3: 0≤x≤0.10, Solid State Commun. 135 (2005) 394–399. doi:10.1016/j.ssc.2005.03.053.

[30] E.M. Anton, W. Jo, D. Damjanovic, J. Rdel, Determination of depolarization temperature of (Bi1/2Na1/2)TiO3-based lead-free piezoceramics, J. Appl. Phys. 110 (2011) 1–14. doi:10.1063/1.3660253.

[31] F. Craciun, C. Galassi, R. Birjega, Electric-field-induced and spontaneous relaxor-

ferroelectric phase transitions in (Na1/2Bi1/2)1 - XBa xTiO3, J. Appl. Phys. 112 (2012). doi:10.1063/1.4770326.

[32] W. Jo, J.E. Daniels, J.L. Jones, X. Tan, P. a. Thomas, D. Damjanovic, J. Rödel, Evolving morphotropic phase boundary in lead-free (Bi1/2 Na1/2)TiO3–BaTiO3 piezoceramics, J. Appl. Phys. 109 (2011) 14110. doi:10.1063/1.3530737.

[33] W. S. Kang, S. K. Lee, J. H. Koh, AC conductivity and dielectric properties of (Bi,Na)0.5TiO3–BaTiO3 lead free ceramics, Ceram. Int. 41 (2015) 6925–6932. doi:10.1016/j.ceramint.2015.01.147.

[34] E. Sapper, S. Schaab, W. Jo, T. Granzow, J. Rödel, Influence of electric fields on the depolarization temperature of Mn-doped (1-x)Bi1/2Na1/2TiO3-xBaTiO3, J. Appl. Phys. 111 (2012) 14105. doi:10.1063/1.3674275.

[35] Z. Yao, R. Chu, Z. Xu, J. Hao, W. Li, G. Li, Processing and enhanced electrical properties of Sr1-x(K0.5Bi0.5)xBi2Nb2O9 lead-free piezoelectric ceramics, Ceram. Int. 42 (2016) 10619–10623. doi:10.1016/j.ceramint.2016.03.156.

[36] S. Zhang, A.B. Kounga, E. Aulbach, W. Jo, T. Granzow, H. Ehrenberg, J. Rödel, Lead-free piezoceramics with giant strain in the system Bi0.5Na0.5TiO3–BaTiO3–K0.5Na0.5NbO3. II. Temperature dependent properties, J. Appl. Phys. 103 (2008) 34108. doi:10.1063/1.2838476.

[37] Q. Xu, D.P. Huang, M. Chen, W. Chen, H.X. Liu, B.H. Kim, Effect of bismuth excess on ferroelectric and piezoelectric properties of a (Na0.5Bi0.5)TiO3-BaTiO3 composition near the morphotropic phase boundary, J. Alloys Compd. 471 (2009) 310–316. doi:10.1016/j.jallcom.2008.03.078.

[38] H. Search, C. Journals, A. Contact, M. Iopscience, (Bi1/2Na1/2) TiO3-BaTiO3 System

for Lead-Free Piezoelectric Ceramics, Jpn. J. Appl. Phys. 2236 (1991) 2236–2239.

[39] M.S. Yoon, N. H. Khansur, S.C. Ur, The effect of pre-milling/pre-synthesis process and excess Ba on the microstructure and dielectric/piezoelectric properties of nano-sized 0.94[(Bi0.5Na0.5)TiO3]-0.06[Ba(1+x)TiO3], Ceram. Int. 36 (2010) 1265–1275. doi:10.1016/j.ceramint.2010.01.011.

[40] Y. Hiruma, K. Yoshii, H. Nagata, T. Takenaka, Investigation of Phase Transition Temperatures on (Bi1/2Na1/2)TiO3-(Bi1/2K1/2)TiO3 and (Bi1/2Na1/2)TiO3-BaTiO3 Lead-free Piezoelectric Ceramics by Electrical Measurements, Ferroelectrics. 346 (2007) 114–119. doi:10.1080/00150190601180471.

[41] X. J. Li, Z. Z. Xi, W. Long, P. Y. Fang, Synthesis of antiferroelectric (Bi0.534Na0.5)0.94Ba0.06TiO3 ceramics with high phase transition temperature and broad temperature range by a solid-state reaction method, Chinese Sci. Bull. 58 (2013) 2893–2897. doi:10.1007/s11434-013-5972-2.

[42] W. Cao, W. Li, T. Zhang, J. Sheng, Y. Hou, Y. Feng, Y. Yu, W. Fei, High-Energy Storage Density and Efficiency of (1− x)[0.94 NBT-0.06 BT]- x ST Lead-Free Ceramics, Energy Technol. 3 (2015) 1198–1204. doi:10.1002/ente.201500173.

[43] P. Fu, Z. Xu, R. Chu, W. Li, G. Zang, J. Hao, Piezoelectric, ferroelectric and dielectric properties of La2O3-doped (Bi0.5Na0.5)0.94Ba0.06TiO3 lead-free ceramics, Mater. Des. 31 (2010) 796–801. doi:10.1016/j.matdes.2009.07.056.

[44] Q. Li, H. Wang, H. Fan, C. Long, X. Liu, Ferroelectric, electromechanical, and dielectric properties of (Na0.5Bi0.5)0.94Ba0.06TiO3 co-doped MnO2 and La2O3 lead-free ceramics, J. Mater. Sci. 49 (2013) 211–217. doi:10.1007/s10853-013-7694-x.

[45] J. Shi, W. Yang, Piezoelectric and dielectric properties of Dy2O3-doped

(Bi0.5Na0.5)0.94Ba0.06TiO3 lead-free ceramics, J. Alloys Compd. 472 (2009) 267–270. doi:10.1016/j.jallcom.2008.04.038.

[46] X. Wang, H.L.W. Chan, C.L. Choy, Piezoelectric and dielectric properties of CeO2-added (Bi0.5Na0.5)0.94Ba0.06TiO3 lead-free ceramics, Solid State Commun. 125 (2003) 395–399. doi:10.1016/S0038-1098(02)00816-5.

[47] Q.C. Peng Fu, Zhijun Xu, Ruiqing Chu, Wei Li, Qian Xie, Yanjie Zhang, Effect of Dy2O3 on the structure and electrical properties of (Bi0.5Na0.5)0.94Ba0.06TiO3 lead-free piezoelectric ceramics, J. Alloys Compd. 508 (2010) 546–553. doi:10.1016/j.jallcom.2010.08.117.

[48] Y.J. Dai, S. Zhang, T.R. Shrout, X.W. Zhang, Piezoelectric and ferroelectric properties of Li-doped (Bi0.5Na0.5)TiO3-(Bi0.5K0.5)TiO3-BaTiO3 lead-free piezoelectric ceramics, J. Am. Ceram. Soc. 93 (2010) 1108–1113. doi:10.1111/j.1551-2916.2009.03535.x.

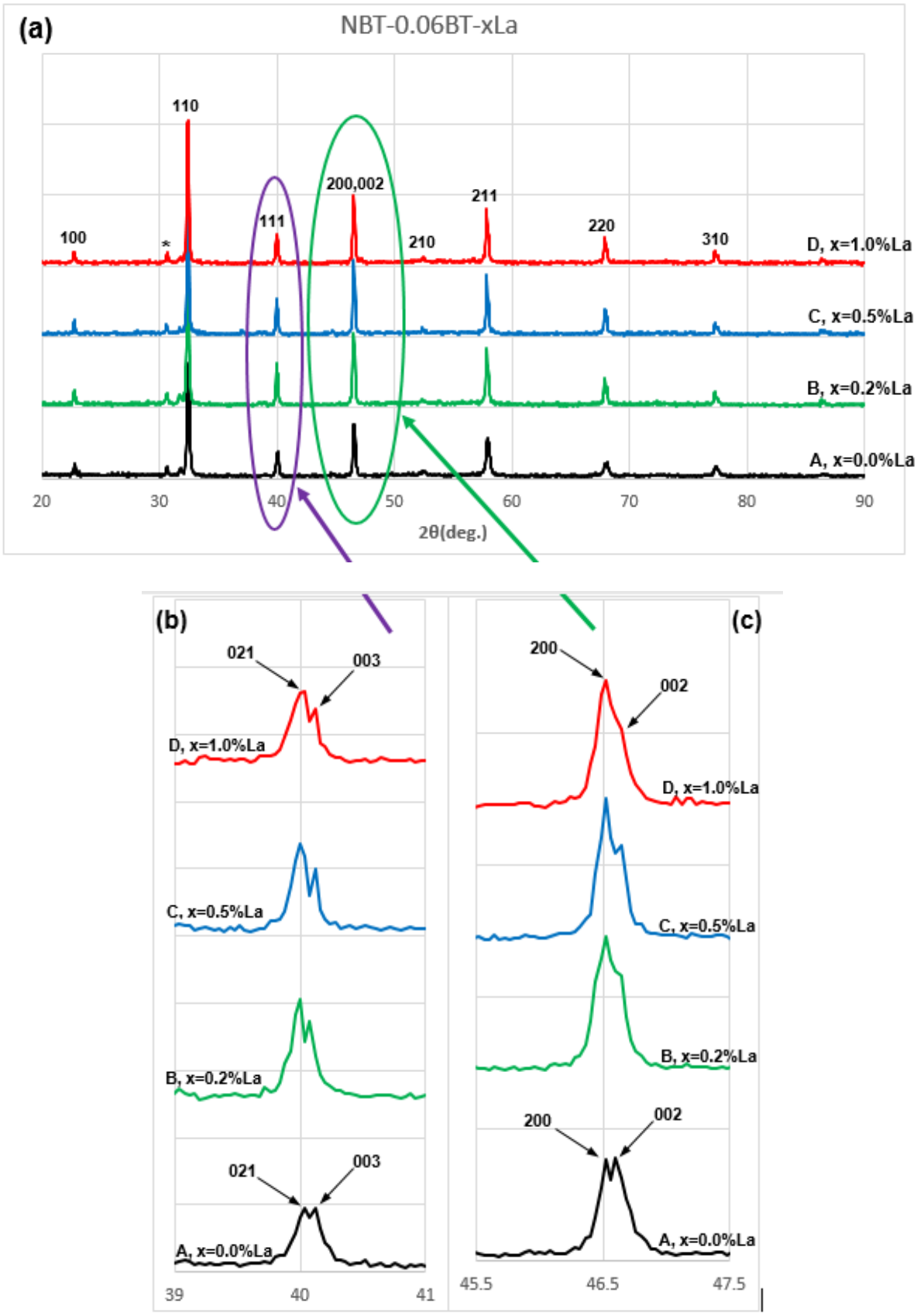
(a)
NBT-0.06BT-xLa
110
200,002
211
111
100
*
210
220
310
D, x=1.0%La
C, x=0.5%La
B, x=0.2%La
A, x=0.0%La
20
30
40
50
60
70
80
90
2θ(deg.)
(b)
021
003
D, x=1.0%La
C, x=0.5%La
B, x=0.2%La
021
003
A, x=0.0%La
39
40
41
(c)
200
002
D, x=1.0%La
C, x=0.5%La
B, x=0.2%La
200
002
A, x=0.0%La
45.5
46.5
47.5

Figure 1

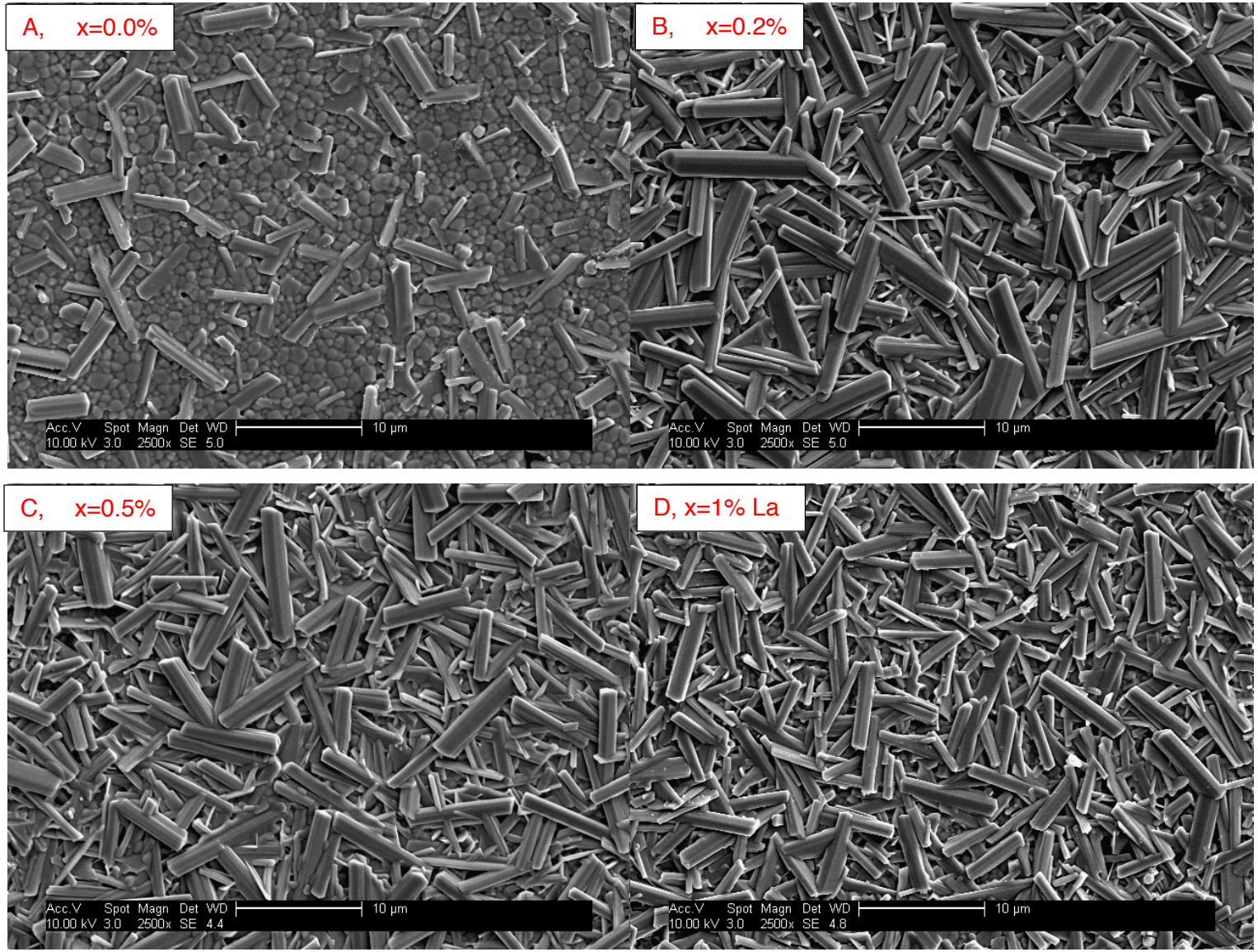
A, x=0.0%
B, x=0.2%
C, x=0.5%
D, x=1% La
Acc.V Spot Magn Det WD
10.00 kV 3.0 2500x SE 5.0
10 µm
Acc.V Spot Magn Det WD
10.00 kV 3.0 2500x SE 5.0
10 µm
Acc.V Spot Magn Det WD
10.00 kV 3.0 2500x SE 4.4
10 µm
Acc.V Spot Magn Det WD
10.00 kV 3.0 2500x SE 4.8
10 µm

Figure 2

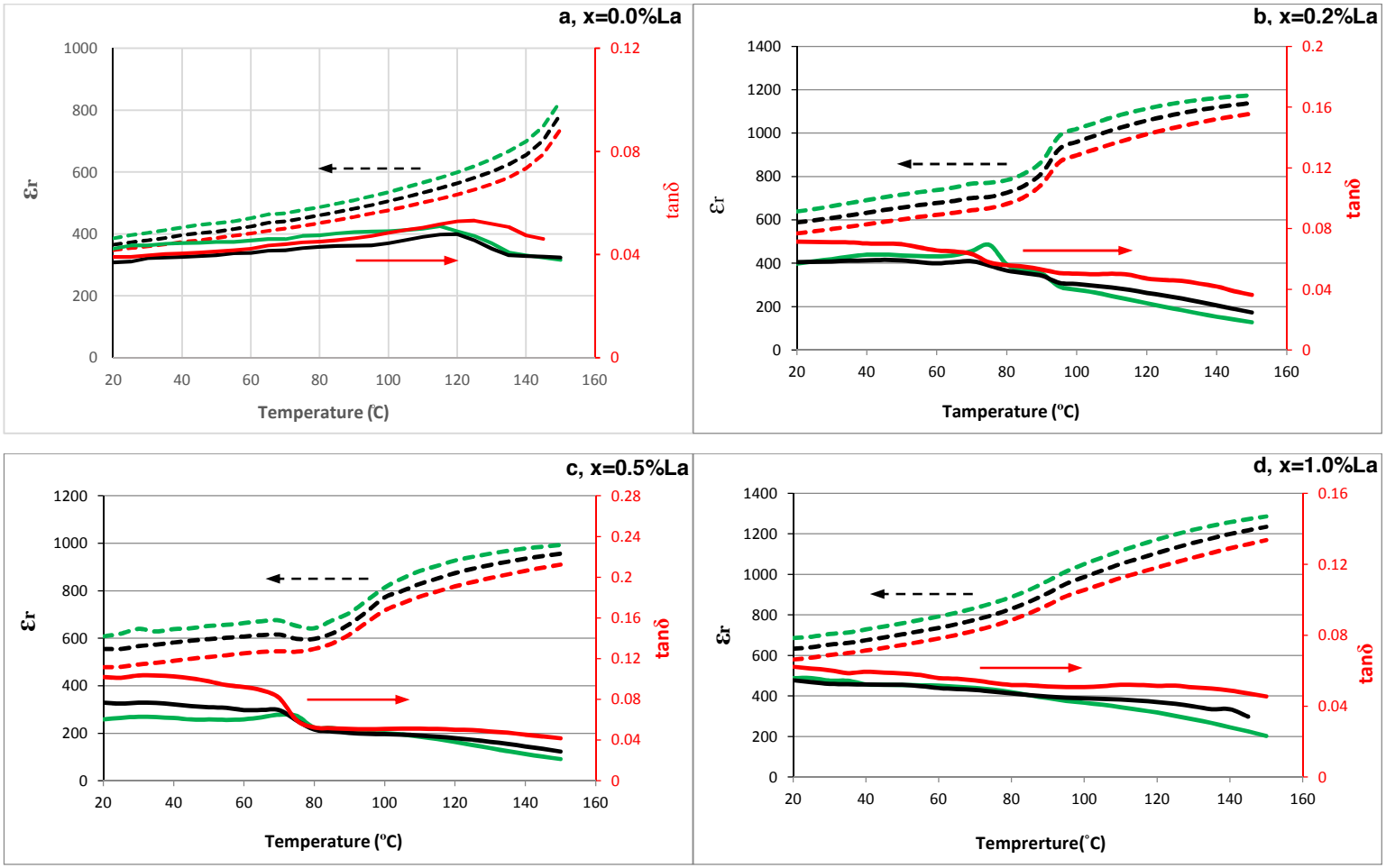
a, x=0.0%La
b, x=0.2%La
c, x=0.5%La
d, x=1.0%La
εr
tanδ
Temperature (℃)
Tamperature (°C)
Temperature (°C)
Temprerture(°C)

Figure 3

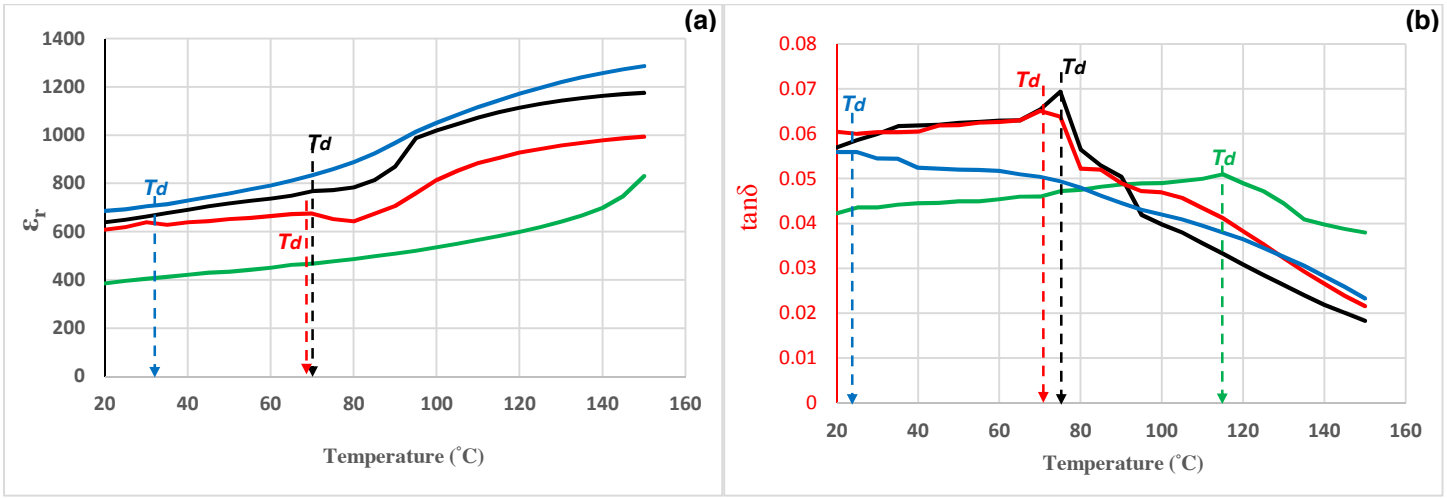
(a)
1400
1200
1000
800
600
400
200
0
ε_r
Td
Td
Td
20
40
60
80
100
120
140
160
Temperature (˚C)
(b)
0.08
0.07
0.06
0.05
0.04
0.03
0.02
0.01
0
tanδ
Td
Td
Td
Td
20
40
60
80
100
120
140
160
Temperature (˚C)

Figure 4

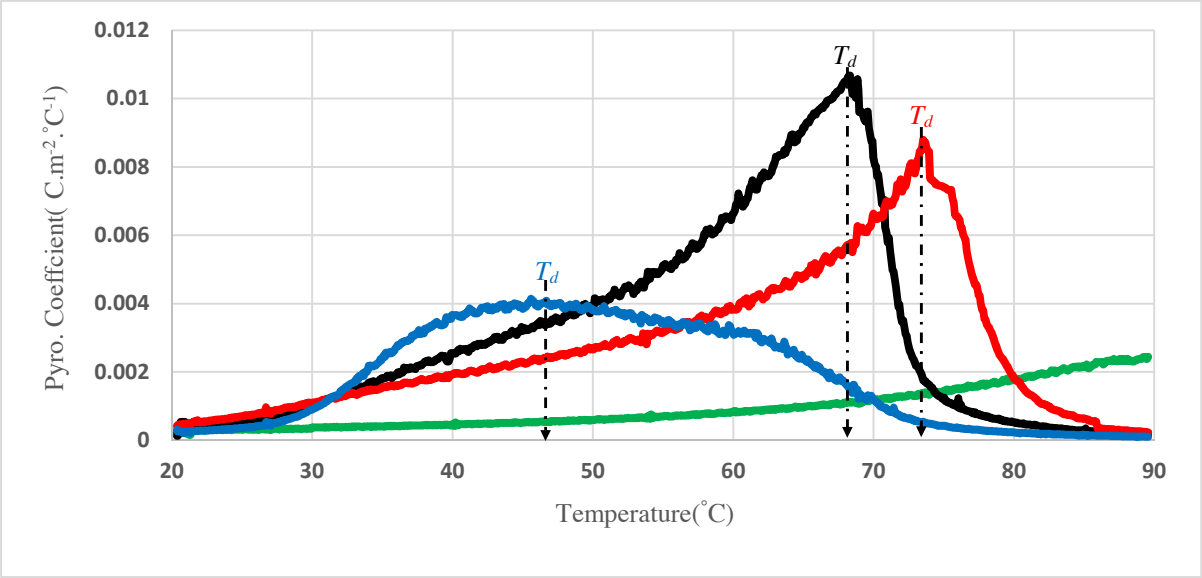
0.012
0.01
0.008
0.006
0.004
0.002
0
Pyro. Coeffcient(C.m-2.˚C-1)
20
30
40
50
60
70
80
90
Temperature(˚C)
Td
Td
Td

Figure 5

NBT-0.06BT-xLa, sample name	Lattice parameter (Å)		c/a ratio
	a	c	
NBT-0.0BT, A	5.5113	13.4744	2.4449
NBT-0.0BT-0.002La, B	5.5178	13.4558	2.4386
NBT-0.0BT-0.005La, C	5.5048	13.5061	2.4535
NBT-0.0BT-0.01La, D	5.4876	13.5114	2.4622

Table 1

Composition	$p\ x10^{-4}\ (C.m^{-2}.^{\circ}C^{-1})$ at *RT*	F_i x10^{-10}(m.V^{-1}) at *RT*	F_v (m^2.C^{-1}) at f. 1kHz at *RT*	F_D x10^{-6}($Pa^{-1/2}$) at f. 1kHz at *RT*	References
NBT-0.06BT	2.14 ± 0.215	1.12 ± 0.437	0.021 ± 0.128	9.08 ± 0.310	This study
NBT-0.06BT-0.002La	5.15 ± 0.331	1.84 ± 0.275	0.032 ± 0.440	1.0 ± 0.115	This study
NBT-0.06BT-0.005La	7.42 ± 0.477	2.65 ± 0.229	0.048 ± 0.439	1.4 ± 0.398	This study
NBT-0.06BT-0.01La	3.60 ± 0.430	1.28 ± 0.391	0.021 ± 0.385	1.4 ± 0.117	This study
PZT	4.14	1.415	0.008	9.01	5,17
NBT-0.07BZT	5.7	2.03	0.0218	10.5	5,17
NBT-0.06BT-0.2Mn	3.5	-	-	-	33
BNKBT	3.25	1.95	0.026	13.43	5,17
KNLNTS	1.9	0.931	0.007	11.5	5,17
NKLBT-0.05BT	3.6	1.27	0.017	-	39

Table 2

Composition	$p\ x10^{-4}\ (C.m^{-2}.^{\circ}C^{-1})$ at 90 ˚C or T_d	$F_i\ x10^{-10}$($m.V^{-1}$) at 90 ˚C or T_d	F_v ($m^2.C^{-1}$) at f. 1kHz at 90 ˚C or T_d	$F_D\ x10^{-6}$($Pa^{-1/2}$) at f. 1kHz at 90 ˚C or T_d	References
NBT-0.06BT	23.9 ± 0.179 at 90 ˚C	8.6 ± 0.416 at 90 ˚C	0.19 ± 0.232 at 90 ˚C	65.5 ± 0.271 at 90 ˚C	This study
NBT-0.06BT-0.002La	105.4 ± 0.320 at 67.9 ˚C	37.6 ± 0.418 at 67.9 ˚C	0.56 ± 0.251 at 67.9 ˚C	18.2 ± 0.210 at 67.9 ˚C	This study
NBT-0.06BT-0.005La	86.1 ± 0.190 at 73.5 ˚C	30.8 ± 0.385 at 73.5 ˚C	0.52 ± 0.249 at 73.5 ˚C	15.8 ± 0.122 at 73.5 ˚C	This study
NBT-0.06BT-0.01La	40.6 ± 0.431 at 46.8 ˚C	14.5 ± 0.189 at 46.8 ˚C	0.22 ± 0.338 at 46.8 ˚C	7.8 ± 0.138 at 46.8 ˚C	This study
NBT-0.07BZT	20.0 at 50 ˚C	7.33 at 50 ˚C	0.066 at 50 ˚C	33.6 at 50 ˚C	5,17
NBT-0.07BZT	22.1 at 87 ˚C	-	-	-	5,17

Table 3

Figures and tables caption:

Figures:

Figure 1: (a) X-ray diffraction patterns of NBT-0.06BT-xLa $0.0 \leq x \leq 1.0$ %; (b) enlargement of splitting [111] peak into [003] and [021] at 39.0° to 41.0°; (c) enlargement of splitting [200] peak into [200] and [002] at 46.0° to 48.0°. * Unidentified peak.

Figure 2: SEM surface morphology of the NBT-0.06BT-xLa $0.0 \leq x \leq 1.0$ (%) ceramics.

Figure 3: Relative permittivity (ε_r) and loss tangent ($tan\delta$) vs temperature for NBT-0.06BT-xLa. a: x = 0.0 %; b: x = 0.2 %; c: x = 0.5 % and d: x = 1.0 %, at three different frequencies (1, 10 and 100) kHz, where εr-1 εr-10 εr-100 tanδ-1 tanδ-10 tanδ-100

Figure 4: (a) the change of the relative permittivity (ε_r) and (b) the loss tangent ($tan\delta$) against temperature (°C) for NBT-0.06BT-xLa , $0.0 \leq x \leq 1.0$ %, from room temperature (*RT*) up to 150°C at 1 KHz and T_d values of all samples where Sample A Sample B Sample C Sample D

Figure 5: Pyroelectric coefficient (p) vs temperature (°C) for the NBT-0.06BT-xLa ceramics, $0.0 \leq x \leq 1.0$ (%), where, Sample A Sample B Sample C Sample D

Tables:

Table 1: The lattice parameters (Å), and c/a ratio for NBT-0.06BT and NBT-0.06BT-xLa (%) compositions.

Table 2: The pyroelectric coefficient and FOM F_i, F_v, and F_D results at room temperature (*RT*) in this study and in literature.

Table 3: The pyroelectric coefficient and FOM F_i, F_v and F_D results at 90°C or depolarization temperature (T_d) in this study and in literature.